Structure of Lennard–Jones nanowires encapsulated by carbon nanotubes*

Wu Wen-Qian(吴雯倩)[a], Tian Ming-Li(田明丽)[b], Chen Hang-Yan(陈航燕)[a], Yuan Qing-Hong(袁清红)[a], and Sun De-Yan(孙得彦)[a]†

[a] *Department of Physics, East China Normal University, Shanghai* 200062, *China*
[b] *College of Electric and Information Engineering, Pingdingshan University, Pingdingshan* 467000, *China*

(Received 8 August 2013; revised manuscript received 23 August 2013; published 2 December 2013)

Molecular dynamics simulations have been performed to investigate the structures of Lennard–Jones (LJ) nanowires (NWs) encapsulated in carbon nanotubes (CNTs). We find that the structures of NWs in a small CNT only adopt multi-shell motifs, while the structures of NWs in a larger CNT tend to adopt various motifs. Among these structures, three of them have not been reported previously. The phase boundaries among these structures are obtained regarding filling fractions, as well as the interaction between NWs and CNTs.

Keywords: structure of nanowires, carbon nanotubes, molecular dynamics simulation

PACS: 61.46.Km, 61.43.Bn, 68.65.–k **DOI:** 10.1088/1674-1056/23/1/016104

1. Introduction

As special one-dimensional systems, nanowires (NWs) filled in carbon nanotubes (CNTs) are of great interest in nanoscience and nanotechnology[1–14] due to their distinct physical and chemical properties. The extremely high chemical and mechanical stability of NWs encapsulated in CNTs ensure that these kinds of materials can be used in various circumstances. Recently, NWs have shown potential applications in heterogeneous catalysis,[1–4] electromagnetic wave absorption,[5,6] high density magnetic data storage devices,[7] sensors for capacitive humidity,[8] oscillators with high frequency,[9,10] etc.

Previous studies have shown that the structure of materials encapsulated in CNTs is very different from that of free-standing materials without any confinement.[15–27] The difference in structure or morphology of confined NWs is primarily due to the elastic energy caused by a mismatch between intrinsic length scale of solid (bond length, lattice constants, etc) and the dimension of confinement space. In order to find the reason for the difference in the structure, it is important to give a convincing description of the elastic energy. Physically, elastic energy is mainly determined by three factors: the number of filling atoms, the radius of CNT, as well as the interaction between NWs and CNTs.[28–35] For example, Xiao *et al.* suggested when the number of Au atoms is large enough, a multi-shell NW will be formed in CNT, otherwise a crystal NW tends to be formed.[29] Choi *et al.* studied the effect of the CNT radius on the structure of encapsulated NWs. They found that, in a small CNT, the stable structure of confined copper was multi-shell packing, while it was face-centered-cubic (fcc) packing as the diameter of CNT increases.[28] Similarly, Zhang *et al.* found that, as the radii of carbon nanotubes increase, the structures of the Ge nanowires transform from a monoatomic chain to helical and multi-shell coaxial cylinders.[35] The effect of interaction strength between the transition metal atom and CNTs has been investigated by using Monte Carlo simulations.[30] The simulation results indicated that the structure of transition metal encapsulated in CNTs was strongly dependent on the interaction strength between metal atoms and CNT. Although much effort has been made, the combined effect of the three major factors on the structure of NWs remains unclear.

In the present work, the structure of Lennard–Jones (LJ) NWs encapsulated in the CNT is investigated by using molecular dynamics (MD) simulations. Three important factors including the number of encapsulated LJ atoms or the filling fractions, the interaction between LJ atoms and CNTs, and the radius of CNTs are considered as a combination to explore their joint effect on the structure of an NW encapsulated in CNTs. Our simulation results show that NWs encapsulated in CNTs with small radius have simple structures, while NWs encapsulated in CNTs with larger radius have various structures. Three new NWs structures encapsulated in CNTs with larger diameter are identified. The phase diagram describing the change of the structure as a function of the number of LJ atoms and the interaction between NWs and CNTs are addressed. In addition, our results also shed light on the structure of a solid confined inside a nanopore.

*Project supported by the National Natural Science Foundation of China (Grant No. 11174079), the National Basic Research Program of China (Grant No. 2012CB921401), and the Shuguang and Innovation Program of Shanghai Education Committee, China.

†Corresponding author. E-mail: dysun@phy.ecun.edu.cn

© 2014 Chinese Physical Society and IOP Publishing Ltd

2. Computational details

Two single-walled CNTs, with indexes of (15,15) and (30,30), are studied. The length of each CNT is about 10 nm. The number of carbon atoms in tube (15,15) and (30,30) are 2460 and 4920, respectively. The periodic boundary condition is only applied along the axial direction, while the free boundary condition is applied along the radial directions. This implies that the system is infinite along the axial direction. Similar to most previous studies,[21,22,28,30] atoms on the CNTs are fixed during the simulation. All LJ atoms are confined only inside CNTs and no atoms are allowed to exist in the region outside of CNTs. The number of LJ atoms ($N_{\rm LJ}$) varies from 1500 to 6000 in (30,30) CNT and from 200 to 1200 in (15,15) CNT. The range of carbon atoms corresponds to a filling fraction varying from 0.2 to 0.75. Here, the filling fraction (γ) is defined as a ratio between the available volume of CNT and the initial volume of NWs with the crystal structure.

The widely used adaptive intermolecular reactive empirical bond order potential with intermolecular interactions[36,37] is adopted to simulate carbon atoms in CNTs. Since we are interested in general results of structure for NWs encapsulated in CNTs, following the previous simulations,[38] the truncated LJ potential[39] is adopted to describe the interatomic interaction of LJ atoms, as well as the interaction between LJ atom and CNT. The LJ parameters among the encapsulated atoms are chosen as $\varepsilon_{\rm ss} = 0.167$ eV and $\sigma_{\rm ss} = 2.314$ Å, which corresponds to the LJ potential for copper.[40] The LJ parameters for carbon–carbon interaction $\varepsilon_{\rm cc} = 0.004555$ eV and $\sigma_{\rm cc} = 3.851$ Å are taken from Ref. [41]. One potential parameter between LJ atoms and carbon atoms ($\sigma_{\rm sc} = 3.805$ Å) is determined by the Lorentz–Lorentz–Berthelot mixing rules,[42] which represents the interaction length scale between carbon and LJ atoms. It is kept unchanged during the whole simulations. The other potential parameter ($\varepsilon_{\rm sc}$), describing the interaction strength between carbon and LJ atoms, is changeable to tune the interaction strength. In present work, three values for $\varepsilon_{\rm sc}$ are chosen to investigate the interaction effect on the structure of encapsulated LJ NWs. The typical value of $\varepsilon_{\rm sc} = 0.02578$ eV is determined by the Lorentz–Berthelot mixing rules.[42] The values of 0.015 eV and 0.035 eV for $\varepsilon_{\rm sc}$ represent the weaker and stronger interaction strength, compared with the typical one.

All MD simulations are performed using large-scale atomic/molecular massively parallel simulator (LAMMPS) package with a time step of 1 fs.[43] The temperature is controlled by Nose–Hoover thermostat.[44,45] The procedure to achieve the equilibrated structure at 0 K is based on the simulated annealing technique. Initially, the system is equilibrated at 1500 K to ensure that the encapsulated atoms are in a well-defined liquid state. Then, the system is cooled down to 0 K with a cooling rate of 1 K/ps. Slower cooling is also adopted to check the cooling rate effect, and we find that final structures keep the same. Hence, we use 1 K/ps in all the simulations to reach a balance between the CPU time and reasonable results. It should be pointed out that, simulation processes are repeated for several times from different initial configurations to minimize the dependence of final configurations on the cooling procedure. For the characterizing of the NW structure, the pair correlation function (PCF) and angle correlation function (ACF) are calculated based on the standard method.

3. Results and discussion

First, we have studied the structure of LJ NWs encapsulated in (15,15) CNT. Simulation results indicate that the NWs adopt multi-shell packing structures in all of the studied cases. The structure of multi-shell NWs includes three coaxial cylindrical shells and a single atom chain located in the center. The structure of each shell is a typical fcc (111) lattice. In order to mathematically define the structure of a multi-shell NW consisting of coaxial shells with n, n', n'', n''' atom rows, Kondo and Takayanagi (KT)[46] developed a KT index $n-n'-n''-n'''$. For the structure of NW confined in tube (15,15), most of the shells in an NW share the same KT index of 16-11-6-1, while the others have 17-12-6-1 KT index. These results are similar to that for the Ge NWs filling into (15,15) CNTs.[35]

For LJ NWs encapsulated in (30,30) CNT, the structure of NWs becomes much more diverse. We have found five structural motifs and three of them are not reported yet. As shown in Fig. 1(a), the first structure motif is labeled as crystal NW, with finite length. The finite length representing the length of NWs is less than that of CNTs. For a typical value of $\varepsilon_{\rm sc}$ ($\varepsilon_{\rm sc} = 0.02578$ eV), the crystal NW is formed only if the filling fraction is small. When the value of $\varepsilon_{\rm sc}$ is equal to 0.015 eV, smaller than the typical one, the crystal NW is formed in a wide range of atom filling fraction. However, by increasing the value of $\varepsilon_{\rm sc}$ to 0.035 eV, the crystal NW disappears for all the studied $N_{\rm LJ}$. Our results suggest that the crystal NW tends to be formed by reducing the strength of the interaction. As the interaction strength between the CNT and NW decreases, the energy increase induced by the mismatch between the nanowire and the CNT wall becomes less and less. This tendency favors the crystal NWs, because the crystal NWs usually have the lowest elastic energy but larger mismatch at interface.

From Fig. 1(a), one can see that the surface atoms in crystal NW exhibit crystalline features, and the cross section becomes fcc (111) lattice. The fcc-type atomic structure of crystal NWs can also be explained from the ACF and PCF shown in Fig. 2. As shown in Fig. 2, main peaks in both ACF and PCF curves are in agreement with the position of the peaks existing in fcc crystals (vertical lines). For the ACF curve,

there are three main peaks centered at 60°, 90°, and 120°, corresponding to the angle distribution peaks (vertical lines) in a pure fcc crystal. In addition, there are other two lower peaks located at 110° and 146°, which can be attributed to the presence of defects in fcc crystals. The angle 110° is caused by twin boundary in a (111) plane, while the other angle 146° in the ACF curve implies the existence of stacking faults. Both of the defects have been reported and well explained by previous studies.[47] Similarly, the PCF also shows some lower peaks close to the position of the main peaks in fcc crystals (vertical lines). Those lower peaks indicate the slight distortion of NWs compared to the typical fcc structure. Interestingly, in a study on the copper nucleation on bending graphene, the authors also found that there is a grain boundary in copper nanostructures.[48]

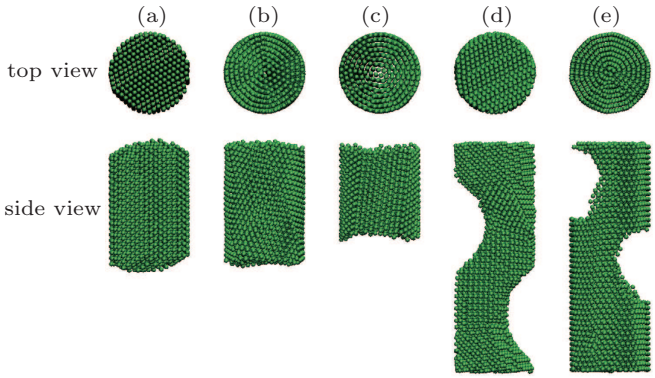


Fig. 1. (color online) Top and side view of five types of NWs encapsulated by (30,30) CNTs, where carbon atoms are not shown. (a) The crystal NW, (b) the multi-shell NW, (c) the hybrid NW, (d) the crystal NW with two droplet-shaped pits on the side (crystal-pit NW), and (e) the multi-shell NW with two droplet-shaped pits on the side (multi-shell-pit NW).

The second structural motif is the so-called multi-shell NW with finite length, as shown in Fig. 1(b). For a smaller ε_{sc} ($\varepsilon_{sc} = 0.015$ eV), we do not find multi-shell NWs by changing the value of N_{LJ}. By increasing the value of ε_{sc} to 0.02578 and 0.035 eV, the multi-shell NW tends to be formed for a larger filling fraction. As shown in Fig. 1(b), the multi-shell NW is composed of eight coaxial cylindrical shells. The spread sheet of each shell is shown in the upper panel of Fig. 3. Each shell exhibits a structure similar to an fcc (111) type lattice. According to the configuration of spread sheets, the KT index of the multi-shell NW is labeled as 43-38-33-28-21-16-10-4. Indeed, multi-shell NWs have been theoretically predicted in many different metals[20–22] and experimentally observed for Au NWs.[26] The ACF and PCF curves of multi-shell NWs (see Fig. 2) clearly show the extended width of each peak distribution. Importantly, the second peak of both ACF and PCF almost disappears, implying the absence of possible defects in the fcc crystal structure. This demonstrates that the multi-shell NWs largely deviate from the fcc-based structure.

The third structural type (labeled as hybrid NW, with finite length) that we find in our current work has not been reported yet. As shown in Fig. 1(c), the LJ atoms near the CNT wall form several shells, while the inner shell shows a crystalline feature. The hybrid NW only exists for the selection of a stronger interaction parameter ($\varepsilon_{sc} = 0.035$ eV) and a lower filling fraction (smaller N_{LJ}). An only similar structure previously reported is the free-standing NWs which were considered as a crystal inner core coated with several outer shells.[17] However, the hybrid NWs inside the CNTs have not been reported previously. The positions of the main peaks in both ACF and PCF (see Fig. 2) are similar to the peak positions in the fcc crystal. Each peak is broadened, indicating the increased distortion compared with the fcc structure. The five outermost sheets in the hybrid NW are extended and shown in the lower panel in Fig. 3. Each shell is composed of both fcc (100) surface (square) and fcc (111) surface (hexagonal). It should be pointed out that, the structures of these shells are very different from the structures of the multi-shell NWs mentioned earlier, which only include the shells composed of fcc (111) surfaces.

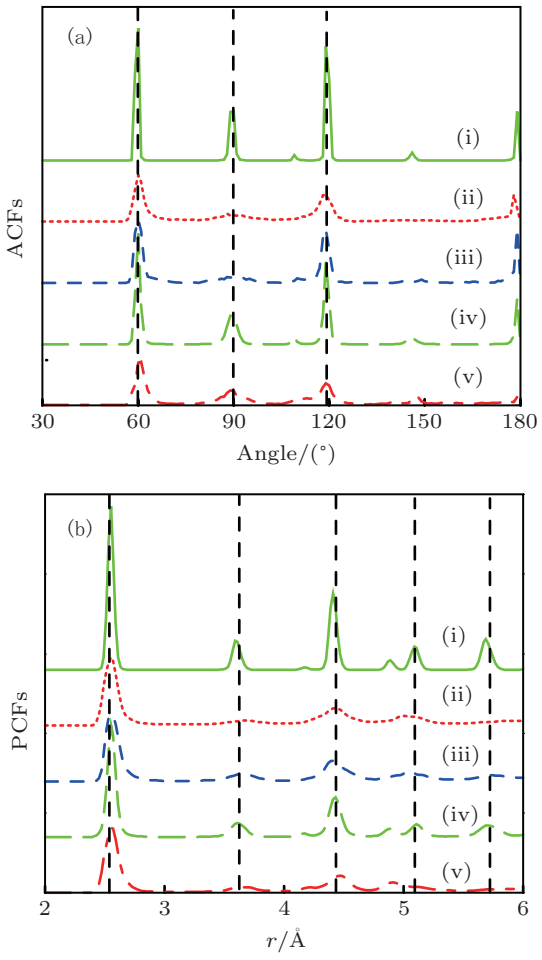


Fig. 2. (color online) (a) The angular correlation functions (ACFs) and (b) the pair correlation functions (PCFs) of five types of NWs encapsulated by (30,30) CNTs. The vertical lines indicate the peak position of prefect fcc crystals. From top to bottom, (i) crystal NW; (ii) multi-shell NW; (iii) hybrid NW; (iv) crystal-pit NW; (v) multi-shell-pit NW.

The forth one, labeled as crystal-pit NW, has the same length as the CNT. This means that the length along the NW axis is infinite because of the periodic boundary conditions. This is also a new NW structure which has not been reported previously. The structure of the crystal-pit NW is very similar to the structure of the crystal NW (see Fig. 1(a)) except for the two droplet-shaped pits near the tube wall. As shown in Fig. 1(d), the top and side view of the crystal-pit NW show crystalline character, although two droplet-shaped pits are formed near the tube wall. The crystal structure of crystal-pit NW is further proved from ACF and PCF curves. As shown in Fig. 2, the main peaks of the ACF and PCF curves in crystal-pit NW agree very well with the peaks in the fcc crystal. The peaks around 110° and 146° indicate that the NW also includes stacking faults. The crystal-pit NW only exists for the selection of the weaker interaction parameter $\varepsilon_{sc} = 0.015$ eV and the largest filling fraction ($N_{LJ} = 5981$, $\gamma = 0.75$).

The last structure type obtained in our study is another newly discovered structure. It is a multi-shell structure with two droplet-shaped pits near the tube wall, labeled as multi-shell-pit NW. The length of the NW remains infinite because of periodic boundary conditions. Without consideration of the droplet-shaped pits, the structure of this NW is similar to the structure of multi-shell NWs discussed earlier (see Fig. 1(b)) because both of them have the same KT index and the similar shape of the ACF and PCF (see Fig. 2) curves. According to the simulation results, the multi-shell-pit NW only exists when the interaction parameter ε_{sc} is equal to a typical value (0.02578 eV) and the filling fraction ($\gamma = 0.75$) is the largest one. It should be pointed out that, if the filling fraction is high enough, both crystal-pit and multi-shell-pit NWs will disappear accordingly.

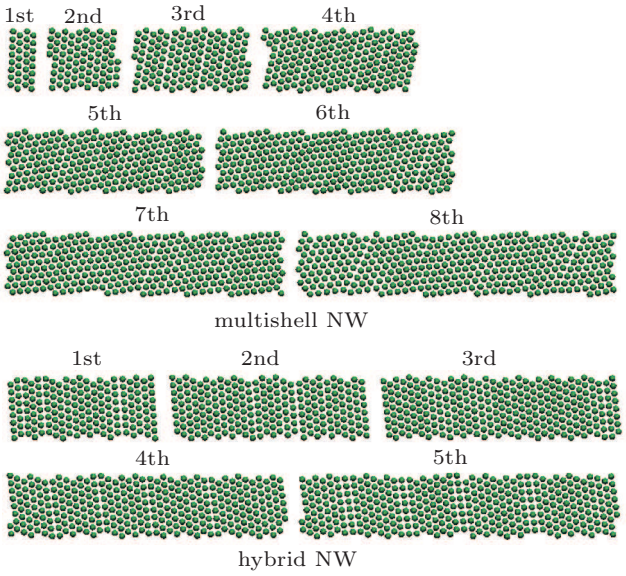


Fig. 3. (color online) Upper panel: the spreading sheets of multi-shell NWs, where the 8th layer refers to the outmost shell. Lower panel: the spreading sheets of hybrid NW, where the 5th layer refers to the outmost shell.

The phase diagram for NWs in (30,30) CNT is summarized in the upper panel of Fig. 4. The results indicate that the stable structure of LJ NWs encapsulated in CNTs strongly depends on N_{LJ} and ε_{sc}. For weaker interaction parameter ($\varepsilon_{sc} = 0.015$ eV), the atoms tend to form an fcc crystal NW in CNTs when N_{LJ} is less than or equal to 5343 corresponding to $\gamma = 0.67$ (filled green square). By increasing the number of atoms N_{LJ}, the crystal-pit NWs are formed when N_{LJ} is equal to 5981 (empty green square). For the typical interaction parameter ($\varepsilon_{sc} = 0.02578$ eV), the crystal NW is formed when N_{LJ} is less than or equal to 3471 corresponding to $\gamma = 0.44$. The multi-shell NW appears when $N_{LJ} \geq 4098$ corresponding to $\gamma = 0.52$. For the multi-shell-pit NW, only if N_{LJ} is equal to 5981, it shows up. When ε_{cs} is selected as a stronger interaction value ($\varepsilon_{cs} = 0.035$ eV), the LJ atoms encapsulated in the CNT form a hybrid NW for $1573 \geq N_{LJ} \geq 2845$ ($0.2 \geq \gamma \geq 0.36$). Then, the hybrid NW turns into multi-shell NW for $N_{LJ} \geq 3471$ ($\gamma \geq 0.44$). For the typical and stronger interaction parameter ($\varepsilon_{sc} = 0.02578$ and 0.035 eV), there is a structure transition between crystal NW/hybrid NW and multi-shell NW. This result is consistent with the previous study which shows that the multi-shell NWs are formed with larger N_{LJ}.[29] After a comparison between two systems with different interaction parameters, we prove that the critical number of atoms related to the structure transition decreases with the increase in interaction parameters.

According to the above analysis, if $N_{LJ}(\gamma)$ or ε_{cs} is small, the interfacial mismatch is not particularly important because of the weak interaction between NW and CNT. The LJ atoms prefer to form the crystal NW when the number of atoms N_{LJ} is small. As $N_{LJ}(\gamma)$ and ε_{cs} increase, the interfacial mismatch becomes significant. Therefore, for the crystal NW, by increasing the number of atoms, the interface energy keeps on increasing until the crystal structure turns into the multi-shell NW to release the extra interface energy. Similarly, for the same value of $N_{LJ}(\gamma)$, with the increase in ε_{cs}, the interface energy increases. In order to release the extra interface energy, the crystal NW turns into the multi-shell NW.

There are two particular cases which involve the competition between the surface energy of NWs and NW–CNT interface energy. This situation occurs at crystal-pit and multi-shell-pit NWs. The structure of crystal-pit and multi-shell-pit NWs is similar to the structure of crystal NW and multi-shell NW. The only difference is that crystal-pit and multi-shell-pit NWs contain two droplet-shape pits on the side of NW, as a compensation to the disappearing surface of NWs by contacting two ends of nanowires to form an infinite NW.

It is worth mentioning that the diameter of CNT does have a great impact on the variety of the structure for the encapsulated NWs. According to the above structure analysis, we find that the structure of NWs in a (30,30) CNT is more

diverse than in a (15,15) CNT. This is possibly due to two reasons. First, the larger inner volume of (30,30) provides more empty spaces for the formation of various structures of the encapsulated NWs. Second, the curvature of (30,30) CNT is fairly smaller than (15,15) CNT, which results in less constrain on the configuration of NWs. In the current study, only the (30,30) CNT and the (15,15) CNT are considered. Even though we do not perform additional calculations for CNTs with larger diameter because of the extremely high computational cost, it is still believed that the structure of NWs in CNT with even larger diameter would be more diverse based on the above structure variety explanations.

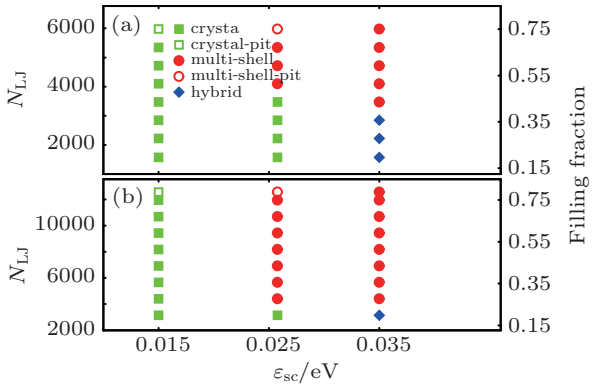


Fig. 4. (color online) The phase diagram for NWs encapsulated by (30,30) CNT, namely, the structure of NWs via the number of LJ atoms (left y axis) or the filling fractions (right y axis) and the interaction between NW and CNT. (a) Length of CNT is 10 nm; (b) length of CNT is 20 nm.

In addition to the tube diameter effect, another interesting question of whether the length of CNT also plays a role in the structure of the encapsulated NWs arises. In order to check this issue, we carry out the structure analysis for the NWs which are encapsulated in a longer (30,30) CNT with the length of about 20 nm. As expected, the obtained trend on 'phase diagram' (the lower panel in Fig. 4) is not changed too much compared with the results for the shorter (30,30) CNT. For each ε_{cs} value, the encapsulated NW structure changes in the same trend for both CNTs with different length. The major difference is the change in the phase boundary. The 'phase boundary' among the crystal, the hybrid, and the multi-shell NWs are irrelevant to the length of the CNT, but only depended on the length of NWs. It can be easily understood that, if the length of NWs is much shorter than the length of the CNT, the change in the tube length could not change the circumstances of NWs, and consequently would not affect the finial structure of the NWs. For the crystal-pit and multi-shell-pit NWs, they only exist when the length of the NW is compatible to the length of the CNT (see Fig. 4). In this case, the change in the tube length only changes the phase boundary of the NWs, but not the structure of NWs itself.

4. Conclusions

We have performed molecular dynamics simulations to study the structure of LJ NWs encapsulated in CNT. The stable structure of LJ NWs confined within CNT varies with the number of LJ atoms, the radius of CNTs, as well as the interaction strength between LJ NWs and CNT. For NWs confined inside (30,30) CNTs, the crystal NW, the hybrid NW, the multi-shell NW, the crystal NW with two droplet-shaped pits near the wall (crystal-pit NW), and the multi-shell NW with two droplet-shaped pits near the wall (multi-shell-pit NW) are found. The phase boundaries among these structures are found to be affected by the interaction between LJ atoms and CNT and the number of LJ atoms. Also, we physically explain the reason for the structure changes in terms of the competition between the elastic energy of NWs and the interface energy between NW and CNT. For (15,15) CNTs, the multi-shell nanowires are the most stable structure among all the cases we studied.

References

[1] Pan X, Fan Z, Chen W, Ding Y, Luo H and Bao X 2007 *Nature* **6** 507
[2] Serp P, Corrias M and Kalck P 2003 *Appl. Catal. A: Gen.* **253** 337
[3] Li W, Liang C, Qiu J, Zhou W, Han H, Wei Z, Sun G and Xin Q 2002 *Carbon* **40** 787
[4] Zheng Q, Zhou W, Qian W, Xiang R, Huang J, Wang D and Wei F 2007 *J. Phys. Chem. C* **111** 14638
[5] Yang Y, Gupta M C, Dudley K L and Lawrence R W 2005 *Nano Lett.* **5** 2131
[6] Liu Z, Bai G, Huang Y, Ma Y, Du F, Li F, Guo T and Chen Y 2007 *Carbon* **45** 821
[7] Sathiya M, Prakash A S, Ramesha K, Tarascon J M and Shukla A K 2011 *J. Am. Chem. Soc.* **133** 16291
[8] Yeow J T W and She J P M 2006 *Nanotechnology* **17** 5441
[9] Kang J W and Hwang H J 2004 *J. Appl. Phys.* **96** 3900
[10] Kang J W, Choi Y G, Lee J H, Kwon O K and Hwang H J 2008 *Mol. Simulat.* **34** 829
[11] Zhao Z F, Li X H, Wen L, Guo H M, Bu S J and Wang Y Q 2012 *Chin. Phys. Lett.* **29** 118103
[12] Liu X, Huang D L, Wu L L, Zhang X T and Zhang W G 2011 *Chin. Phys. B* **20** 078101
[13] Zhang L N, He J, Zhou W, Chen L and Xu Y W 2010 *Chin. Phys. B* **19** 047306
[14] Li D Z and Zhu R 2013 *Chin. Phys. B* **22** 018502
[15] Wang B, Wang G and Zhao J 2002 *Phys. Rev. B* **65** 235406
[16] Zhuo G and Gao Q 2005 *Solid State Commun.* **136** 32
[17] Wang B, Yin S, Wang G, Buldum A and Zhao J 2001 *Phys. Rev. Lett.* **86** 2046
[18] Hui L, Wang B, Wang J and Wang G 2004 *J. Chem. Phys.* **121** 8990
[19] Shao J, Yang C, Zhu X and Lu X 2010 *J. Phys. Chem. C* **114** 2896
[20] Arcidiacono S, Walther J H, Poulikakos D, Passerone D and Koumoutsakos P 2005 *Phys. Rev. Lett.* **94** 105502
[21] Kang J W and Hwang H J 2004 *Physica B* **351** 144
[22] Kang J W and Hwang H J 2004 *Nanotechnology* **15** 115
[23] Wang S, Zhang Y, Chen L, Zhang J and Xu K 2011 *Phys. Stat. Sol. (a)* **1** 97
[24] Zhu B, Wang Y, Pan Z, Cheng D and Hou M 2010 *Eur. Phys. J. D* **57** 219
[25] Takagi D, Homma Y, Hibino H, Suzuki S and Kobayashi Y 2006 *Nano Lett.* **6** 2642
[26] Díaz M, Costa-Krämer J L, Medina E, Hasmy A and Serena P A 2003 *Nanotechnology* **14** 113
[27] Qiao Z J, Chen G D, Ye H G, Wu Y L, Niu H B and Zhu Y Z 2012 *Chin. Phys. B* **21** 087101
[28] Choi W Y, Kang J W and Hwang H J 2003 *Phys. Rev. B* **68** 193405

[29] Xiao Y, Zhu B, Guo S, Wang Y and Pan Z 2009 *Nucl. Instrum. Meth. Phys. Res. B* **267** 3067
[30] Gou J Y and Xu C X 2011 *Appl. Phys. A* **102** 333
[31] Li K, He H, Xu B and Pan B 2009 *J. Appl. Phys.* **105** 054308
[32] Guo Y, Kong Y, Guo W and Gao H 2004 *J. Comput. Theor. Nanosci.* **1** 93
[33] Yang W, Nelissen K, Kong M, Zeng Z and Peeters F M 2009 *Phys. Rev. E* **79** 041406
[34] Piacente G, Schweigert I V, Betouras J J and Peeters F M 2004 *Phys. Rev. B* **69** 045324
[35] Zhang X Q, Li H and Liew K M 2007 *J. Appl. Phys.* **102** 073709
[36] Stuart S J, Tutein A B and Harrison J A 2000 *J. Chem. Phys.* **112** 6472
[37] Brenner D W, Shenderova O A, Harrison J A, Stuart S J, Ni B and Sinnott S B 2002 *J. Phys.: Condens. Matter* **14** 783
[38] Guo Y and Guo W 2006 *Nanotechnology* **17** 4726
[39] Broughton J Q and Gilmer G H 1983 *J. Chem. Phys.* **79** 5095
[40] Cleri F, Yip S, Wolf D and Phillpot S R 1997 *Phys. Rev. Lett.* **79** 1309
[41] Rappe A K, Casewit C J, Colwell K S, Goddard W A and Skiff III W M 1992 *J. Am. Chem. Soc.* **114** 10024
[42] Allen M P and Tildesley D J 1987 *Computer Simulation of Liquids* (Oxford: Clarendon)
[43] Plimpton S J 1995 *J. Comput. Phys.* **117** 1
[44] Nose S 1984 *J. Chem. Phys.* **81** 511
[45] Hoover W G 1985 *Phys. Rev. A* **31** 1695
[46] Kondo Y and Takayanagi K 2000 *Science* **289** 606
[47] Kang J W and Hwang H J 2002 *J. Phys.: Condens. Matter* **14** 2629
[48] He Y, Li H, Li Y, Zhang K, Jiang Y and Bian X 2013 *Phys. Chem. Chem. Phys.* **15** 9163